STM JOURNALS

Journal of
Experimental & Applied Mechanics

ISSN: 2230-9845 (Online)
ISSN: 2321-516X (Print)
Volume 16, Issue 1, 2025
January–April
DOI (Journal): 10.37591/JoEAM

https://journals.stmjournals.com/joeam

Research JoEAM

A Finite Element Analysis to Study the Effect of Hydrostatic Pressure on Steel Ductility

Tapas Kumar Datta[1,*]

Abstract

The effect of superimposed hydrostatic pressure on percentage reduction of area (a gauge mark of the ductility) is investigated in round steel bars in tensile stress by employing a finite element analysis (FEA) with 8-node serendipity quadrilateral elements and von Mises plasticity flow rule in an elastoplastic power law hardening model. It is demonstrated that a linear relationship exists between the pressure and percentage reduction of area at any given value of percentage elongation varying from 0.15 to 0.456 with step increase of 0.05. This finding by the finite element analysis is in consonance with the experimental finding by a research work that the plot of the ratio of the area of the tensile part of the break to the total area as a function of pressure is roughly linear and that there is no evidence that the linear relation between pressure and ductility will cease to hold at pressures higher than that were reached in the experiments.

Keywords: Ductility, finite element analysis (FEA), hydrostatic pressure, von Mises plasticity flow rule, elastoplastic, power law hardening

INTRODUCTION

Hydrostatic pressure can affect metals in a number of ways – it can increase the shear strength of metals, can also increase the ductility and fracture strain of sheet metal. It is generally accepted that the superimposed hydrostatic pressure increases fracture strain of sheet metals [1]. The studies of Bridgman [2], Weir et al. [3], and Spitzig and Richmond [4] on many metals show that pressure increases the strength substantially. For example, Bridgman's tests found that the flow stress for tempered pearlite at a strain of 2.75 increased from 1.758 GPa at atmospheric pressure to 2.171 GPa when pressurized to approximately 2.482 GPa. Rauch et al. [5] also have concluded that superimposed hydrostatic pressure increases the yield and flow stress of the martensitic AISI 4330 steel.

Similarly, Brownrigg et al. [6] have found that the flow stress of spheroidized 1045 steel increases linearly with superimposed hydrostatic pressure, whereas Spitzig and Richmond [4] have concluded on the basis of their results on iron-based material that although the flow stress is a linear function of hydrostatic pressure, the plastic dilatancy is negligible, and is, therefore, not related to the flow rule of von Mises. Spitzig [7] informed that the data available for polycrystalline bcc crystals and alloys tested under superimposed hydrostatic pressure are inconclusive because with increase in pressure either small or no change in flow stress has been observed.

It has been shown by Bridgman [8–10] that ductility of a material increases when subjected to tension with superimposed hydrostatic pressure. It is shown for steel, Bridgman [8], that as the hydrostatic pressure is increased from the normal atmospheric pressure to 2.68 GPa, the character of fracture is also altered from the normal cup and cone fracture to rupture at a point.

***Author For Correspondence**
Tapas Kumar Datta
E-mail: tapaskdatta@gmail.com

[1]An Alumnus, Department of Metallurgical Engineering, Indian Institute of Technology, Kharagpur, West Bengal, India

Received Date: December 21, 2024
Accepted Date: January 14, 2025
Published Date: January 20, 2025

Citation: Tapas Kumar Datta. A Finite Element Analysis to Study the Effect of Hydrostatic Pressure on Steel Ductility. Journal of Experimental & Applied Mechanics. 2025; 16(1): 41–51p.

Bridgman [8] has considered that the external pressure tends to prevent the formation of internal cracks from which fracture might be initiated, and experimental tests from tensile tests under superimposed hydrostatic pressure, Thomason [11], confirm that micro void nucleation is virtually eliminated as the pressure reaches a magnitude of the order of the uniaxial yield stress, *Y*, whereas Lian and Suery [12] referring to a work of one of them, have this to say that cavity growth is completely suppressed for pressures greater than about one-third of the tensile stress. As per Dieter [13], compressive hydrostatic stresses close up small pores or separation at phase interfaces and make fracture propagation difficult, but since hydrostatic pressure cannot exert shear stress, it does not influence the number of dislocations in a pile-up – the reason for that the hydrostatic stress affects crack propagation, not initiation.

Thomason [11] has summarized the effect of a fluid hydrostatic pressure on the ductile fracture process in tensile specimens stating that a large fluid hydrostatic pressure enhances ductility by suppressing the nucleation, growth and coalescence of micro voids, all the three stages in the ductile fracture process.

It has been pointed out that even brittle material becomes ductile at sufficiently high pressure, and the beneficial effect of hydrostatic pressure has been used to work upon brittle materials such as bismuth and cast iron [13].

It is also pointed out by Dieter [13] that hydrostatic pressure does not affect tensile instability of metals. While deliberating upon the effect of pressure on tensile plastic instability, Alexander [14] has considered it reasonable to suppose, on the basis that hydrostatic pressure has no effect on yielding behavior, that hydrostatic pressure would also have no effect on the initiation of necking. It is stated in Thomason [11] that it has been shown theoretically by Hill [15] and confirmed experimentally by French and Weinrich [16–18] that the bifurcation strain at incipient necking remains same for all magnitudes of hydrostatic pressure. The study by Korbel et al. [19] on Al-Zn-Mg alloy indicates that the onset of localization is not sensitive to the applied pressure.

In conclusion, hydrostatic pressure does not affect the flow stress and creates less damage to the material [13].

ELASTIC-PLASTIC CONSTITUTIVE RELATIONSHIP

To evaluate how metal deformation, ductility etc. can be predicted by a finite element program, it is but necessary to begin with plasticity theory. For this, three requirements are [20]:

1. Under elastic condition, that is, before onset of plastic deformation, a stress-strain relationship, namely, $\{\sigma\} = [D]^{elastic}\{\epsilon\}$ be known ([D]-matrix/constitutive matrix contains material property indices);
2. For 'elastic breakdown' [21], when plastic yielding starts, a yield criterion or yield function, *f*, to indicate stress level at the start of plastic yielding, be postulated; in general, a yield function for isotropic material, of same properties in all directions, is written: f(σ_1 , $\sigma_2, \sigma_3 = 0$; this equation represents a surface in the space of principal stress σ_i and when the stress state as a point is inside the surface, the material behaviour is elastic, and when the stress state as a point is on the surface, then the material is yielding, but a stress state outside the surface is not possible to be attained, Britto and Gunn [21]; for metals, the past-suggested yield criteria, other than Tresca criterion and von Mises criterion, conflict with experimental findings and are only of historic interest [20]. The experimental results show that actual yield points fall between the Tresca and von Mises predictions and close to the latter [22]. Neilsen and Schreyer [23] stress that the Tresca model does not predict the generation of necking in metals, and is, therefore, not appropriate for metals showing necking, and that the von Mises plasticity model captures the variation in bifurcation (necking, the transition from uniform to non-uniform deformation) mode, and is capable of predicting a wide range of features observed experimentally in a number of metals.

The von Mises yield criterion (1913) says that plastic yielding starts when J_2, the second deviatoric stress invariant [equal to $\frac{1}{3}(I_1^2 - 3I_2)$ where I_1 and I_2 denote the first and second invariants of the stress tensor with $I_1 = \sigma_1 + \sigma_2 + \sigma_3$, $I_2 = \sigma_1\sigma_2 + \sigma_2\sigma_3 + \sigma_3\sigma_1$, the σ_i representing the principal stress] reaches a critical value, *k*, rather, when $\sqrt{J_2} = k$, or, $\sqrt{3}\sqrt{J_2} \equiv \sqrt{I_1^2 - 3I_2} = \sqrt{3}\,k$, or, $\sqrt{3}\sqrt{J_2} \equiv \sqrt{\frac{(\sigma_1-\sigma_2)^2+(\sigma_2-\sigma_3)^2+(\sigma_3-\sigma_1)^2}{2}} = \sqrt{3}k$, or, $\overline{\sigma} = \sqrt{3}k$, (1)

where $\sqrt{3}\sqrt{J_2}$, denoted by $\overline{\sigma}$, is called the effective stress, generalized stress or equivalent stress [20] for the uniaxial case, $\sigma_1 = \sigma$ and $\sigma_2 = \sigma_3 = 0$, $\overline{\sigma} = \sigma$, that is, in uniaxial tension ($\sigma_2 = \sigma_3 = 0$) the von Mises criterion requires that $\sqrt{3}\,k$ is the uniaxial yield stress *Y* [20].

In other words, $f_{VM} \equiv \sqrt{3}\sqrt{J_2} - Y = 0$ (Smith [24]). (2)

Also Smith [24]: $J_2 = \frac{1}{6}\{(\sigma_x - \sigma_y)^2 + (\sigma_y - \sigma_z)^2 + (\sigma_z - \sigma_x)^2\} + \tau_{xy}{}^2 + \tau_{yz}{}^2 + \tau_{zx}{}^2]$

3. When the material is yielding plastically, that is, for post-yield behavior, with both elastic and plastic components of deformation, a relationship between stress and strain must be developed; here, the relationship is expressed in terms of, to note, increments of stress and strain, that is,

$\{d\sigma\} = [D^{ep}]\{d\epsilon\}$, (3)

$[D|\quad|ep]$ is the elastic-plastic [D]-matrx, tangent stiffness matrix, and $\{d\epsilon\} = \{d\epsilon^{el}\} + \{d\epsilon^{pl}\}$ and $d\epsilon^{pl}\ \lambda\frac{\partial g}{\partial\{\sigma\}}$, (4)

That is, the plastic strain increment is proportional to the strain gradient of plastic potential *g*, λ being the proportionality constant, termed plastic multiplier, its theoretical basis developed in Hill [25]. The last equation, Equation (4), is termed the 'flow rule', it governs the plastic flow after yielding. Using the 'flow rule' and yield function, *f*, by some manipulation [20, 22, 24], a formula for $[D^{ep}]$ can be obtained as below:

$$= [D] - \frac{[D]\frac{\partial g}{\partial\{\sigma\}}\left(\frac{\partial f}{\partial\{\sigma\}}\right)^T[D]}{A + \left(\frac{\partial f}{\partial\{\sigma\}}\right)^T[D]\frac{\partial g}{\partial\{\sigma\}}} \quad (5)$$

where $[D] \equiv$ matrix, *g* and *f* are the flow surface and yield surface respectively, and *A* is the shift of the yield surface which is called the plastic modulus (work hardening) that can be determined experimentally from a uniaxial test, being the local slope of the uniaxial stress-plastic strain curve [20], and for the 'perfect' plasticity, *A* is 0 [24]. *A* is positive or negative for strain hardening or strain softening materials, respectively.

NUMERICAL IMPLEMENTATION

In the present analysis, the material behavior under multiaxial loading condition is predicted by a generalization of the uniaxial power law relationship. Here, using the uniaxial power law expression $\sigma_1 = K.\epsilon_1^N$, *K* and *N* the hardening modulus and hardening exponent, respectively, the plastic modulus, *A* is equal to $\frac{E.\frac{d\sigma_1}{d\epsilon_1}}{E-\frac{d\sigma_1}{d\epsilon_1}}$, as given in Owen and Hinton [20], or, $A = \frac{E.(K.N.\epsilon_1{}^{N-1})}{E-(K..N.\epsilon_1{}^{N-1})}$, and the strain hardening slope at any given state of stress and strain is:

$$A = \frac{E.\left(K.N.\bar{\epsilon}^{N-1}\right)}{E-\left(K..N.\bar{\epsilon}^{N-1}\right)}, \quad (6)$$

by extrapolating the uniaxial curve to $\overline{\sigma} = K.\bar{\epsilon}^N$, for more general state of stress, $\overline{\sigma}$ ($= \sqrt{3}\sqrt{J_2}$) and effective strain or equivalent strain, $\overline{\epsilon}$ ($= \frac{\sqrt{2\{\epsilon_r - \epsilon_\theta|\quad|+(\epsilon_\theta - \epsilon_z) + (\epsilon_z - \epsilon_r)\}+3\gamma_{rz}{}^2}}{3}$), for axisymmetric state of stress.

It has been reported by Rajendran and Bless [26] that *A*, the instantaneous hardening slopes/tangent moduli can be found using known uniaxial stress-strain data. The data for *K* and *N*, however, being not readily available, Equation (6) as such is unable to give the value for *A*.

It is considered that necking initiates on the attainment of load maximum, and condition for necking is $\varepsilon \geq N$ for a material with the stress-strain relationship, $\sigma = K\varepsilon^N$ [27]. But a correct determination of the true strain ε at the maximum load may not be easy for steel due to its flat curve near the maximum load [28]. Dieter [3] mentions about the difficulty as to establishing the strain at maximum load from the flat engineering stress-strain curve near the point of necking. Metwalli et al. [29] reported nearly 13% difference in the value of *N* between the automated image processing and test machine records.

In the present finite element analysis (FEA), the expression for *K*, $K = {\sigma_Y}^{1-N}.E^N$, as in Tuğcu et al. [30], or,

$K = {s_Y}^{1-N}.E^N$ ($\because \sigma_Y \cong s_Y$, yield strength, YS), (7)

and that for ultimate tensile strength (UTS), s_u Dieter [3], as $s_u = K.\left(\frac{N}{e}\right)^N$ where e = 2.718, lead to:

$$s_u = (E^N.{s_y}^{1-N})\left(\frac{N}{e}\right)^N = (E^N \frac{s_Y}{{s_Y}^N})\left(\frac{N}{e}\right)^N \text{ , or } \frac{s_u}{s_Y} = \left(\frac{E}{e.s_Y}\right)^N . N^N \quad (8)$$

The above Equation (8) gives the value for *N*, the hardening exponent, from the known and readily available values for Young's modulus, *E*, yield strength (YS), s_Y (or *Y*), and ultimate tensile strength (UTS), s_u, and then the value for *K* is found from Equation (7), and finally the value for plastic modulus, *A*, is found from Equation (6), from the calculated values of *K* and *N* (and $\overline{\epsilon}$).

However, Equation (8) cannot give the value for *N* explicitly as a function of s_u and s_Y, and a program as given below has been prepared to get the value for *N* from the given values of s_u and s_Y:

```
C     Subroutine SUBNV(E,EN,HARMOD,SB,SU)
C
C        A program for calculating hardening exponent, N
C
C     DOUBLE PRECISION
C    1      E,EN,HARMOD,SB,SU
      REAL   E,EN,HARMOD,SB,SU
C     OPEN (95,FILE = 'nkoutput',STATUS = 'OLD')
C
      E = 2.E11
C     WRITE(*,*) 'GIVE VALUE OF EN:'
C     READ(*,*) EN
C
     SU = 3.61E8
     SB = 2.19E8
C     WRITE(*,*) 'GIVE VALUE OF SU:'
C     READ(*,*) SU
C     WRITE(*,*) 'GIVE VALUE OF SB:'
C     READ(*,*) SB
C
      IF ( ((SU-SB)/SB).LT..1) THEN
        EN = .0
        GO TO 2
     END IF
```



```
C
      C2 = LOG(SU/SB)
      C1 = LOG(E/(EXP(1.)*SB))
      EN = .0
C
      IF ( ((SU-SB)/SB).LE..33) ENINC = .01
      IF ( ((SU-SB)/SB).GT..33) ENINC = .1
C     ENINC = .01
C
C     WRITE(*,*) 'GIVE VALUE OF ENINC AND ISTOP'
C     READ(*,*) ENINC,ISTOP
      ISTOP = 35
      LN = 1
      LNN = 1
    1 CONTINUE
      IF (LN.GT.ISTOP.OR.LNN.GT.ISTOP) THEN
         WRITE  ( *,99)
         WRITE  (23,99)
   99    FORMAT (////'Change the value/s of `ENINC" and/or `ISTOP" in
     1 the subroutine/program `SUBNV".')
         STOP
      END IF
      EN = EN + ENINC
      CLHS = C2/(C1+LOG(EN))
      RHS = EN
      WRITE( *,*) 'EN = ',EN,' LHS = ',CLHS,'  RHS = ',RHS
C     WRITE(95,*) 'EN = ',EN,' LHS = ',CLHS,'  RHS = ',RHS
      IF ((CLHS-RHS).GT.1.E-8) THEN
C     IF ((CLHS-RHS).GT.0.) THEN
         LN = LN + 1
         IF (LN.EQ.1) ENINC = -(ENINC/10.)
         LNN = 0
         IF (ABS(CLHS-RHS).GT.1.E-8) GO TO 1
                     ELSE
         LNN = LNN + 1
         IF (LNN.EQ.1) ENINC = -(ENINC/10.)
         LN = 0
         IF (ABS(CLHS-RHS).GT.1.E-6) GO TO 1
       END IF
    2 HARMOD = (E**EN) * (SB**(1-EN))
C     WRITE(95,*) 'HARMOD = ', HARMOD
      WRITE(*,*) 'HARMOD = ', HARMOD
C     RETURN
      STOP
      END
```

For the given values of $E = 2.0 \times 10^{11}$ Pa, $s_u = 3.61 \times 10^8$ Pa and $s_Y = 2.19 \times 10^8$ Pa, the program gives the value for N as 0.13 and that for K as 5.38×10^8 Pa.

With the values of K, and N known and A calculated from Equation (6), the elastic-plastic [D] matrix can be found from Equation (5), if $\frac{\partial g}{\partial\{\sigma\}}$ and $\frac{\partial f}{\partial\{\sigma\}}$ are known.

When the plastic potential function is same as the yield function, that is, $g = f$, what is achieved is called the 'associated flow'. In reference [21] it says that according to Hill [25], it is likely that there is a relation between the plastic potential g and function f, and that $g = f$ appears to be true for metals. Therefore, for associated flow, Equation (5) needs value for $\frac{\partial f}{\partial\{\sigma\}}$ only, which is [31],

$\frac{\partial f}{\partial\{\sigma\}} = \frac{\partial f}{\partial J_2}\cdot\frac{\partial J_2}{\partial\{\sigma\}} = \frac{\sqrt{3}}{2\sqrt{J_2}}\cdot\frac{\partial J_2}{\partial\{\sigma\}} = \frac{3}{2\acute{\sigma}}\cdot\frac{\partial J_2}{\partial\{\sigma\}}$, and therefore, using the expression for J_2 from Equation (2),

$$\frac{\partial f}{\partial\sigma_x} = \frac{3}{2\acute{\sigma}}\cdot\frac{\partial J_2}{\partial\sigma_x} = \frac{3}{2\acute{\sigma}}\cdot\cdot\frac{2\sigma_x-\sigma_y-\sigma_z}{3}, \frac{\partial f}{\partial\sigma_y} = \frac{3}{2\acute{\sigma}}\cdot\frac{\partial J_2}{\partial\sigma_y} = \frac{3}{2\acute{\sigma}}\cdot\frac{2\sigma_y-\sigma_z-\sigma_x}{3}, \quad (9)$$

$\frac{\partial f}{\partial\sigma_z} = \frac{3}{2\acute{\sigma}}\cdot\frac{\partial J_2}{\partial\sigma_x} = \frac{3}{2\acute{\sigma}}\cdot\frac{2\sigma_z-\sigma_x-\sigma_y}{3}, \frac{\partial f}{\partial\tau_{xz}} = \frac{3}{2\acute{\sigma}}\cdot\frac{\partial J_2}{\partial\tau_{xz}} = \frac{3}{2\acute{\sigma}}.)$,

where, for axisymmetric stresses, $\sigma_r \equiv \sigma_x$, $\sigma_z \equiv \sigma_z$, $\tau_{rz} \equiv \tau_{xz}$, and $\sigma_\theta \equiv \sigma_y$.

So, with known elastic [D] matrix, all the terms may be evaluated to work with Equation (3), the incremental stress-strain relation. While von Mises yield criterion may be used for metals, for rock, soil etc., Drucker Prager and Mohr-Coulomb criteria are in use.

RESULTS AND DISCUSSION

The present analysis does not make prediction as to when a bar breaks as it has not investigated into the fracture or voids or damage of the material. But, the analysis is to find out if the superimposed pressure itself puts any influence on the material's ductility, the percentage reduction of area, %RA (= $\frac{R_0^2-R^2}{R_0^2}\times 100$) for a given elongation (= $\frac{L-L_0}{L_0}$); for the necking stress state, $R \equiv R_{min}$. Other than the applied hydrostatic pressure, on the bar's cylindrical side, the numerical tensile simulation details for axisymmetric round bar are same as provided in Datta [32]. Only 8-noded quadrilateral elements are used in this analysis.

For this analysis, the effect of variation in yield strength, YS, and ultimate tensile strength, UTS, on %RA for a given elongation, 0.456, the largest employed in the present analysis, is first studied. Using the values of YS, UTS, and Young's modulus, E (= 200 GPa), the K and N values are first calculated and then the FEA are carried out to get the simulated necked profiles of the bar and %RA values at normal atmospheric pressure as displayed in Table 1. Throughout the analysis R_0= 0.006 m, $L_0/2$ = 0.025, that is, L_0/D_0, the initial length/diameter ratio of the bar is 4.17, and the Poisson's ratio, ν, is assumed to be 0.3. The first row of Table 1 refers to a low-carbon steel as provided in Dieter [13], from which YS = [24.8/($\pi 6^2$) = 0.219 GPa], UTS = [24.8/($\pi 6^2$ = 0.361 GPa], average Young's modulus, E = [(Load/A_0)/($\Delta L/L_0$) 200 GPa] are calculated. It is readily seen from Table 1 that the material ductility, %RA remains unaffected, at roughly 77%, even as YS and UTS vary in a wide range.

Table 1. Effect of yield strength (YS) and ultimate tensile strength (UTS) on percentage reduction of area (%RA) (for given elongation, 0.456).

YS (10^8 Pa)	UTS (10^8 Pa)	K (10^8 Pa)	N	%RA
2.19	3.61	5.38	0.13	76.98
	4.61	7.53	0.18	
	5.61	9.74	0.22	
	6.61	11.99	0.25	76.97
	7.61	14.29	0.28	
	8.61	16.63	0.30	76.96
	9.61	7.537–18.99	0.1–0.32	
1.19	3.61	6.32	0.22	76.98
0.19		6–7.77	0.40	

Table 2. Tensile bar simulation to find *R* and percentage reduction in area (%RA) with variation of elongation.

Elongation	R_{min} (m) of simulated neck	%RA
0.294	3.99	55.83
0.314	3.85	58.81
0.356	3.56	64.73
0.386	3.36	68.68
0.456	2.88	76.98

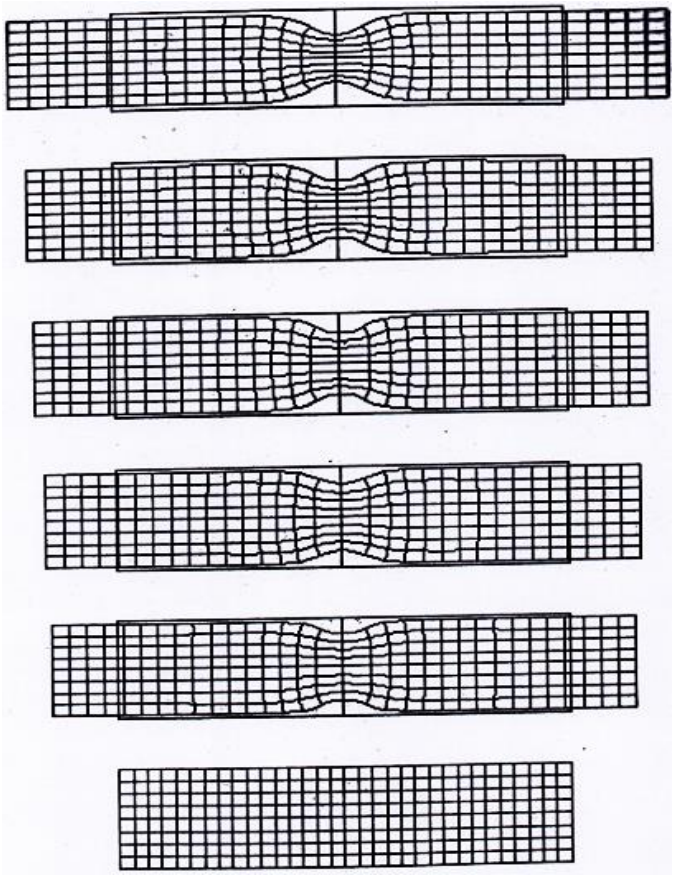

Figure 1. Post-instability profile of a round bar at elongations 0.294, 0.314, 0.356, 0.386, and 0.456.

It is necessary to find prior to undertaking the study of the application of hydrostatic pressure, how the tensile bar simulates in the post-bifurcation stage, with the progressive increment of elongation. The result of this study has been incorporated in Table 2 (the test data as in Dieter [13] viz., 3.15 and 72.44, respectively, are comparable with the simulation find as in the last row). The simulated profiles of the neck look as in Figure 1.

In Figure 1, the leftmost mesh picture is for the round tensile bar with radius R_0 as received, and then the progressive elongations picture the neck progression. The radius of the necked bar at the middle is R_{min} ($\equiv R$) from which %RA is calculated, as given in Table 1.

The next two tables, Table 3 and 4, present the computational results of the FEA that demonstrate the effect of superimposed hydrostatic pressure on the %RA. Based on these results, Figures 2 and 3 are drawn. When the data from Table 3 are plotted in Figure 2, it is seen that %RA increases linearly with the superimposed hydrostatic pressure when necking is in progress.

Table 3. Progress of percentage reduction in area (%RA) with hydrostatic pressure, for given elongation.

Pressure *(GPa)*	%RA at the given Elongation						
	0.15	***0.2***	***0.25***	***0.3***	***0.35***	***0.4***	***0.456***
Nil	31.29	40.43	48.91	56.7	63.9	70.4	76.98
1.0	33.63	42.55	50.87	58.54	65.6	71.9	78.29
2.0	35.88	44.71	52.88	60.40	67.3	73.4	79.56
3.0	38.10	46.75	54.77	62.13	68.8	74.9	80.90
4.0	40.24	48.76	56.61	63.82	70.4	76.3	82.09

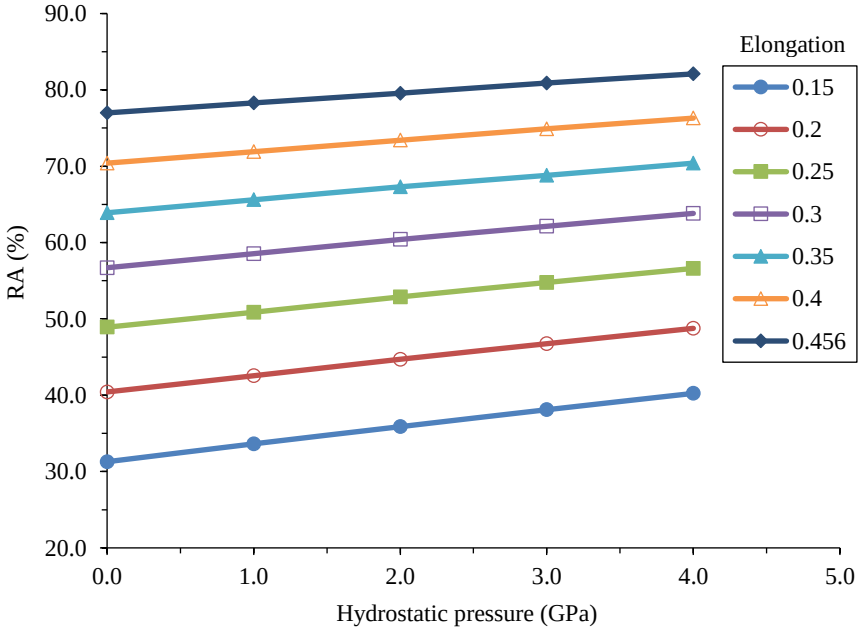

Figure 2. Effect of hydrostatic pressure on the percentage reduction in area (%RA) on a round bar, for given elongation.

Table 4. Progress of percentage reduction in area (%RA) with elongation, superimposed hydrostatic pressure.

Pressure (GPa)	%RA at the Given Elongation							
	0.15	***0.2***	***0.25***	***0.3***	***0.35***	***0.4***	***0.45***	***0.5***
Nil	31.29	40.43	48.91	56.74	63.91	70.4	76.3	76.98
1.6	33.63	42.55	50.87	58.54	65.56	71.9	77.7	82.72
2.6	37.20	45.94	54.02	61.44	68.22	74.3	79.8	84.51
3.6	39.38	47.96	55.88	63.15	69.76	75.7	80.3	85.68

The data of Table 4 are plotted in Figure 3, it is seen that the nature of variation of %RA with elongation, roughly linear, remains same with the superimposed hydrostatic pressure as with nil superimposed hydrostatic pressure. Only, the difference in %RA, between the values at 3.6 GPa and nil hydrostatic pressure, at lower elongation is slightly higher, about 8%, at elongation 0.15 (when necking has not set in) compared to about 5% at elongation 0.5 (when the necking has much set in).

The effect of superimposition of hydrostatic pressure, up to 4 GPa, on the neck diameter at the given elongation 0.456 (Table 4) is seen in Figure 4. Whereas the %RA at atmospheric pressure is 76.98, at the superimposed pressure of 4.0 GPa, it is 82.09, that is, there is an increase of about 6.6% [{(82.09 – 76.98)/76.98}× 100], for the material analyzed in the present study, namely, a low-carbon steel.

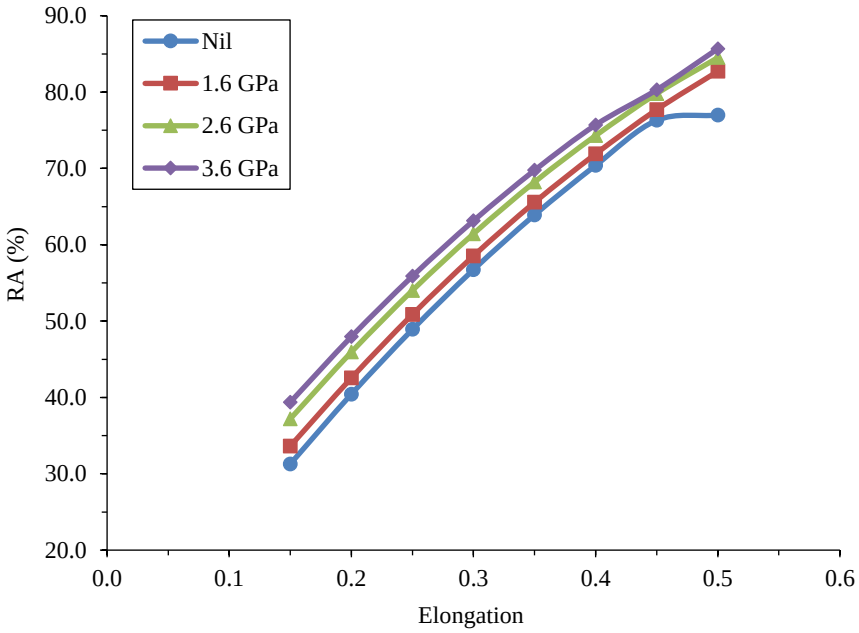

Figure 3. Progress of percentage reduction in area (%RA) with elongation, for given pressure, on a round bar.

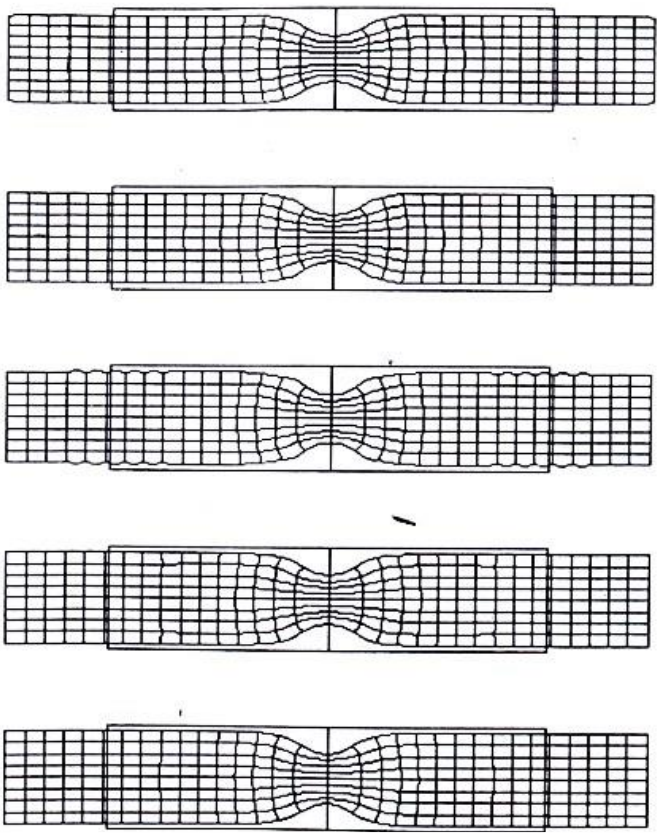

Figure 4. Effect of superimposed hydrostatic pressure, nil to 4 GPa, on the neck of a round bar.

The numerical results above indicate to that even in the absence of micro-voids, the superimposition of hydrostatic pressure is expected to contribute to increase in ductility since at all elongations %RA is seen to increase when hydrostatic pressure is superimposed.

CONCLUSION

The effects of superimposed hydrostatic pressure on the %RA, a measure of material ductility, has been studied numerically by finite element analysis in steel round bars under tension employing von Mises strain-hardening plasticity model and associated flow. The work is brought to a closure with the conclusions as below:

1. Only the readily available elastic constants, Young's modulus, E, Poisson's ratio, ν, and the strength data, yield stress, YS, and the tensile strength, UTS, are required for the present analysis. These data are sufficient for calculation of the hardening exponent, N, the hardening modulus, K, and the plastic modulus, A.
2. The material ductility, %RA remains unaffected even with wide variation in YS and UTS.
3. The numerical results indicate to that even in absence of micro-voids superimposition of hydrostatic pressure is expected to contribute to enhanced ductility since for all elongations %RA is seen to increase when hydrostatic pressure is superimposed.
4. The %RA increases linearly with the superimposed hydrostatic pressure when necking is simulated, as Figure 2 shows.
5. The nature of variation of %RA with elongation remains same with the superimposed hydrostatic pressure as with the 'nil' hydrostatic pressure (Figure 3).

REFERENCES

1. Shahzamamian M, Thomsen C, Partovi A, Xu Z, Wu P. Numerical study about the influence of superimposed hydrostatic pressure on shear damage mechanism in sheet metal, Metals. 2021; 11 (8): 1193.
2. Bridgman PW. The effect of hydrostatic pressure on plastic flow under shearing stress. J Appl Phys. 1946; 17 (8): 692–698.
3. Weir SW, Akilla J, Ruddli C, Goodwin T, Siemy L. Static strength of Ta and U under ultrahigh pressure. Phys Rev B. 1998; 57: 11258–11265.
4. Spitzig WA, Richmond G. The effect of pressure on the flow stress of metals. Acta Metall. 1984; 32 (3): 457–463.
5. Rauch GC, Daga RL, Radcliffe SV, Sobir RJ, Leslie WP. Volume expansion, pressure effects, and the strength differential in as quenched iron-carbon martensite. Metall Trans A. 1975; 6A: 2279–2287.
6. Brownrigg A, Spitzig WA, Richmond G, Teirlinck D, Embury JD. The influence of hydrostatic pressure on the flow stress and ductility of a spheroidized 1045 steel. Acta Metall. 1983; 3 (3): 1141–1150.
7. Spitzig WA. Effect of high hydrostatic pressure on the plastic properties of iron single crystals. Acta Metall. 1979; 27: 523–534.
8. Bridgman PW. Effect of high hydrostatic pressure on the plastic properties of metals. Rev Mod Phys. 1945; 17: 3–14.
9. Bridgman PW. The tensile properties of several special steels and certain other materials under pressure. J Appl Phys. 1946; 17: 201–212.
10. Bridgman PW. Studies in Large Plastic Flow and Fracture With Special Emphasis on the Effects of Hydrostatic Pressure. Cambridge, MA, USA: Harvard University Press; 1964.
11. Thomason PF. Ductile Fracture of Metals. Oxford, UK: Pergamon Press; 1990.
12. Lian J, Suery M. Effect of strain rate sensitivity and cavity growth rate on failure of superplastic material. Mater Sci Technol. 1986; 2 (11): 1693–1698.
13. Dieter GE. Mechanical Metallurgy. London, UK: McGraw-Hill Book Company; 1988.
14. Alexander JM. The effect of pressure on tensile plastic instability – a fallacious argument. J Inst Metals. 1964–1965; 93: 366–367.
15. Hill R. The Mathematical Theory of Plasticity. Oxford, UK: Oxford University Press; 1964.
16. French IE, Weinrich PF. The influence of hydrostatic pressure on the tensile fracture of α-brass. Acta Metall. 1973; 21: 1533–1537.
17. French IE, Weinrich PF. The influence of hydrostatic pressure on the tensile deformation of a 0.5 C steel. Scripta Metall. 1974; 8: 87–90.

18. French IE, Weinrich PF. The influence of hydrostatic pressure on the tensile deformation and fracture of copper. Metall Trans A. 1975; 6A: 785–789.
19. Korbel A, Raghunathan VS, Teirlinck D, Spitzig W, Richmond O, Embury JD. A structural study of the influence of pressure on shear band formation. Acta Metall. 1984; 32: 511–519.
20. Owen DRJ, Hinton E. Finite Elements in Plasticity: Theory and Practice. Swansea, UK: Pineridge Press Limited; 1980.
21. Britto AM, Gunn MJ. Critical State Soil Mechanics via Finite Elements. Chichester, UK: Ellis Horwood Limited Publishers; 1987.
22. Chen WF, Han DJ. Plasticity for Structural Engineers. New York, NY, USA: Springer-Verlag; 1988.
23. Neilsen MK, Schreyer HL. Bifurcation in elastic-plastic materials. Int J Solids Struct. 1993; 30: 521–544.
24. Smith IM. Programming the Finite Element Method with Application to Geomechanics. Chichester, UK: John Wiley & Sons; 1982.
25. Hill R. The Mathematical Theory of Plasticity. Oxford, UK: Oxford University Press; 1950.
26. Rajendran AM, Bless SJ. Determination of tensile flow stress beyond necking at very high strain rate. Exp Mech. 1986; 26: 319–323.
27. Semiatin SL, Jonas JJ. Formability & Workability of Metals – Plastic Instability 7 Flow Localization. Metals Park, OH, USA: American Society for Metals; 1984.
28. Gao Y, Wagoner RH. A simplified model of heat generation during the uniaxial tensile test, Metall Trans A. 1987; 18A: 1001–1009.
29. Metwalli SM, Ragab AR, Kanel AH, Abdul Saheb A. Determination of plastic stress-strain behavior by digital-image-processing techniques. Exp Mech. 1987; 27: 414–422.
30. Tuğcu P, Neale KW, Lahoud AQ. Inertial effects on necking in tension. Int J Solids Struct. 1990; 11: 1275–1285.
31. Zienkiewicz OC. The Finite Element Method. 3rd edition. New Delhi, India: Tata McGraw Hill Publishing Company; 1979.
32. Datta TK. Computation of the necking in bars without geometrical imperfection. Int J Fracture Mech Damage Sci. 2024; 2 (2): 10–19.

